

Calibrated real-time detection of nonlinearly propagating strain waves

André Bojahr,¹ Marc Herzog,¹ Daniel Schick,¹ Ionela Vrejoiu,² and Matias Bargheer^{1,3,*}

¹*Institute of Physics and Astronomy, University of Potsdam, Karl-Liebknecht-Strasse 24-25, 14476 Potsdam, Germany*

²*Max-Planck-Institut für Mikrostrukturphysik, Weinberg 2, 06120 Halle, Germany*

³*Helmholtz Zentrum Berlin, Albert-Einstein-Str. 15, 12489 Berlin, Germany*

(Received 19 July 2012; revised manuscript received 2 October 2012; published 24 October 2012)

Epitaxially grown metallic oxide transducers support the generation of ultrashort strain pulses in SrTiO₃ (STO) with high amplitudes up to 0.5%. The strain amplitudes are calibrated by real-time measurements of the lattice deformation using ultrafast x-ray diffraction. We determine the speed at which the strain fronts propagate by broadband picosecond ultrasonics and conclude that, above a strain level of approx. 0.2%, the compressive and tensile strain components travel at considerably different sound velocities, indicating nonlinear wave behavior. Simulations based on an anharmonic linear-chain model are in excellent accord with the experimental findings and show how the spectrum of coherent phonon modes changes with time.

DOI: [10.1103/PhysRevB.86.144306](https://doi.org/10.1103/PhysRevB.86.144306)

PACS number(s): 43.35.+d, 43.25.+y, 61.05.cp, 63.20.kg

Acoustic wave propagation and the deformation of solids are usually analyzed within the approximation of harmonic interatomic potentials leading to the concept of decoupled acoustic phonons including their dispersion relation which is nearly linear for small wave vectors k_P . An anharmonicity must be introduced into the interaction potential in order to describe deformation under very high stress. But also small-phonon-amplitude phenomena are connected to phonon-phonon interaction processes, such as heat expansion and heat conduction.¹ For the material investigated in this paper, SrTiO₃ (STO), all these properties have been studied in detail, since STO is the generic dielectric (quantum paraelectric) perovskite oxide with a variety of interesting properties near its structural phase transition at 105 K. The elastic constants were determined by ultrasound measurements,² the damping of acoustic phonons was investigated by the linewidth of Brillouin scattering³ and apparent deviations of the acoustic dispersion were discussed in the context of picosecond ultrasonics measurements.⁴ Recently ultrafast x-ray diffraction (UXRD) was used to accurately measure the propagation and decay of quasimonochromatic strain pulses in STO.⁵ In general, UXRD data yield unambiguous information on the ultrafast lattice response, which is helpful for the interpretation of optical pump-probe investigations concerning complex problems in solids.^{6–8}

In theory, the changes in the occupation of phonon modes are described as phonon damping due to scattering from defects or anharmonic interaction with thermally activated phonons.^{9–12} For high strain amplitudes also interactions among coherent phonons are possible, which leads to a shape change of coherent phonon pulses. In particular, the self-steepening of strain pulses in sapphire giving rise to N-waves, shock waves, and soliton pulse trains were measured after a long propagation length of more than one hundred microns.^{13–16} These solitons were observed at low temperatures where phonon damping is weak and were discussed by nonlinear wave equations.^{16–18}

In this paper we investigate the nonlinear propagation of giant longitudinal acoustic (LA) bipolar strain pulses in SrTiO₃. We calibrate the strain amplitude by UXRD and show how the mode spectrum constituting the wave changes

as a function of time. Simulations based on an anharmonic linear-chain model yield excellent agreement with ultrashort broadband optical reflectivity measurements and show that compressive strain components propagate faster than tensile strain components. The dependence of the sound velocity on the strain gives rise to a self-steepening of the strain fronts. We analyze the experiments in a linear-chain model with atomic resolution, although for the presented results a continuum model would also be applicable. There are several advantages of this approach and the discussion of sound waves in terms of phonons. First we anticipate experiments for very high wave vectors approaching the Brillouin zone boundary. At a temperature of 110 K, STO undergoes an antiferrodistortive phase transition connected to an optical phonon mode which softens near the zone boundary.¹⁹ For connecting the nonlinear parameters derived in the present paper with the physics near the phase transition our approach will be very helpful. Finally, ultrafast x-ray diffraction naturally supports simulations with unit cell accuracy, and we show in Eq. (1) that in our picosecond ultrasonics experiments the different wavelengths of the reflected photons are sensitive to particular wave vectors of phonons.

We use an epitaxially grown La_{0.7}Sr_{0.3}MnO₃ (LSMO) transducer film on a SrTiO₃ (001) substrate, fabricated by pulsed-laser deposition. The red symbols in Fig. 1(a) show a θ - 2θ scan of the sample recorded at the energy dispersive reflectometer (EDR) beamline of the synchrotron BESSYII of the Helmholtz-Zentrum-Berlin. The bright substrate peak at $\theta = 23.25^\circ$ is cut off to show the less intense layer peak (LSMO) at 23.58° more clearly. The excellent agreement with the simulation (black solid line) confirms the crystalline perfection of the epitaxial film with a thickness of $d_{\text{LSMO}} = 36$ nm, which is very robust against high excitation densities and supports high strain amplitudes. To calibrate the amplitude of the strain wave we measure the expansion of the metallic layer via the shift of the x-ray diffraction signal [Figs. 1(b) and 1(c)] after optical excitation by 50 fs laser pulses around 800 nm wavelength with a fluence of 20 mJ/cm². To probe the structural dynamics we use an x-ray plasma source which provides jitter-free x-ray pulses with a duration of approximately 200 fs.²⁰ The transient angular shift $\Delta\theta$ of the

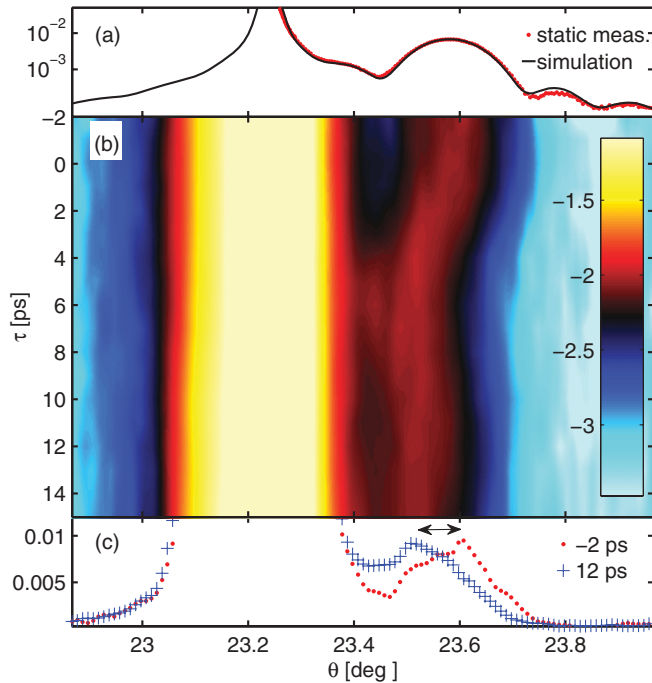


FIG. 1. (Color online) (a) Static θ - 2θ scan of the (002) peaks of the LSMO-STO sample showing a weak and broad layer (LSMO) peak and a much brighter and narrower STO substrate peak. (b) Transient UXRD signal after pumping with a laser pulse. The layer peak shifts to smaller angles indicating the expansion of LSMO within 6 ps (logarithmic color code). (c) Two cuts of panel (b) with pump-probe delays -2 ps (before pumping) and 12 ps (when the strain pulse has left the layer).

LSMO Bragg peak can be read from Fig. 1(b) for time delays up to 15 ps. The shift is connected to the layer strain ϵ by Bragg's law. Figure 1(c) shows the diffraction curve for a time delay of 12 ps yielding an induced LSMO strain of $\epsilon = 0.2\%$.

The observed time dependence of the LSMO Bragg peak can be understood as follows:^{21,22} The absorbed pump pulse induces a quasi-instantaneous thermal stress which is unbalanced at the layer boundaries. This leads to two strain fronts which propagate away from the air-LSMO and LSMO-STO interfaces eventually building up a bipolar strain pulse in the STO substrate.²³ The maximum expansion occurs at $T = d_{\text{LSMO}}/v_{\text{LSMO}} = 6$ ps after the excitation, when the expansion waves starting from the surface and the interface have traveled through the film at the velocity of sound in LSMO, v_{LSMO} .²⁴ After 12 ps the coherent strain wave has completely left the LSMO layer and entered the STO substrate. Reflections of the sound wave at the interface with good acoustic impedance matching can be neglected.^{21,24,25}

In previous experiments we confirmed that the layer strain depends linearly on the excitation fluence²⁶ and that the corresponding bipolar strain wave propagates into the STO substrate.²¹ Hence we conclude a calibration factor of 0.01% LSMO strain per 1 mJ/cm^2 fluence. The strain amplitude of the bipolar pulse in the STO is half of the LSMO strain after 12 ps weighted with the ratio of the layer and substrate sound

velocities which considers the bipolar pulse stretching in the STO.^{21,24,25}

Having calibrated the amplitude of the lattice response, we follow the propagation of the bipolar strain pulse by optical pump-probe measurements. The setup is very similar to the broadband picosecond ultrasonics setup reported by Pontecorvo *et al.*²⁷ We split the 800 nm laser light into two parts. The intense part is used to pump the sample with fluences ranging from 14 to 47 mJ/cm^2 and the smaller part is focused into a sapphire plate to generate a white light supercontinuum pulse. This spectrally broad light pulse ranging from 470 to 700 nm is reflected from the sample under an angle $\alpha = 45^\circ$ with respect to the surface normal. We measured the relative transient reflectivity change $\Delta R/R_0$ of the sample for four different fluences at pump-probe delays up to 1 ns with a resolution of 1 ps. Figure 2 shows the response of the sample after correction for the chirp of the white light probe pulse and after subtraction of the slowly varying background which is associated with the transient heat in the LSMO film. Figure 2(a) shows the relative change of reflectivity for the lowest fluence (14 mJ/cm^2) and Fig. 2(b) shows the same for the highest fluence (47 mJ/cm^2).

All measurements show pronounced oscillations which exhibit a period increasing with the probe wavelength λ . At high fluences we additionally observe a wavelength-dependent beating of these oscillations. The oscillations can be understood as an interference of the light wave reflected by the sample surface with the light wave reflected due to

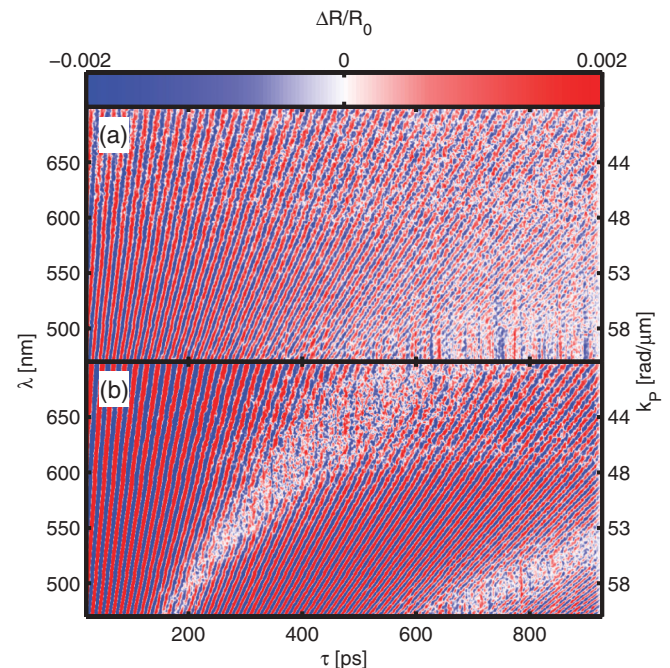


FIG. 2. (Color) Relative optical reflectivity change of the LSMO-STO sample for a pump fluence of (a) 14 mJ/cm^2 and (b) 47 mJ/cm^2 . The low-frequency background was subtracted by high pass filtering. The probe pulse wavelength is given by λ (left axis). Both measurements show oscillations which are attributed to Brillouin backscattering of a photon from a phonon with wave vector k_p (right axis). For strong excitation conditions (b) we observe a beating in these oscillations.

the refractive index change induced by the propagating strain wave.²³

In order to explain how a photon with wave vector k_L is selectively probing a certain phonon with wave vector k_P , we describe the propagating wave front as a superposition of longitudinal acoustic (LA) phonons with wave vector k_P . Then the “reflection” of the probe light from the strain pulse can be understood as Brillouin backscattering of optical light with wave vector k_L . Therefore, such oscillations are often denoted as “Brillouin oscillations” in the literature.²⁸ The observed frequency ω_P of the signal oscillation corresponds to the eigenfrequency of the LA phonon with wavevector k_P . According to energy and momentum conservation the latter is related to the probe wavelength λ by the Brillouin backscattering condition

$$k_P = 2k_L^\perp = \frac{4\pi}{\lambda}n(\lambda)\cos(\beta), \quad (1)$$

where k_L^\perp is the internal optical wave vector component along the surface normal and $n(\lambda)$ is the refractive index of STO which is taken from the literature.²⁹ The internal angle β is related to α by Snell’s law. Equation (1) implies that the probe wavelength is specific for a certain wave vector of LA phonons. The amplitude of oscillations at each wavelength λ and time interval is a measure of the phonon amplitude of a specific phonon wave vector k_P . The beating observed in Fig. 2(b) is therefore interpreted as a change of the phonon spectrum in time. In particular, the beat node indicates the absence of a certain wave vector k_P at a certain time delay after excitation. This will be discussed in the context of Fig. 4.

Now we discuss how to derive the sound velocity from the measured data shown in Figs. 2(a) and 2(b). The linear dispersion relation of acoustic phonons near the Brillouin zone center is given by $\omega_P(\lambda)/k_P = v_s$ and thus relates the observed oscillation frequency $\omega_P(\lambda)$ to the speed of sound v_s for the LA phonons in STO:

$$v_s = \frac{\omega_P(\lambda)\lambda}{4\pi n(\lambda)\cos(\beta)}. \quad (2)$$

We then calculate the fast Fourier transform $I(\omega_P, \lambda)$ along the time axis for each probe wavelength λ . This yields a relation between λ and the related oscillation frequencies $\omega_P(\lambda)$, which implies a dependence of the sound velocity v_s on the phonon wave vector k_P according to the Brillouin backscattering condition. We use Eq. (2) as a coordinate transformation $v_s(\omega_P(\lambda), \lambda)$ which transforms our Fourier-transformed data into a wavelength-dependent sound velocity distribution $I(v_s, \lambda)$. By integration of the calculated result over all wavelengths we obtain Fig. 3, which shows the measured sound velocity distributions for different photoinduced LSMO strains calibrated by the results of the UXRD measurement. At low strain (0.14%) we observe a single peak around 8 nm/ps which is in a good agreement with the known sound velocity of the LA phonons in STO.²⁵ This peak validates the linear dispersion at low fluence. A nonlinear dispersion (k_P -dependent sound velocity) would lead to a broadened distribution.

However, with increasing strain amplitude we find a splitting in the sound velocity distribution. This implies that, for large strains, the speed of sound depends on the strain

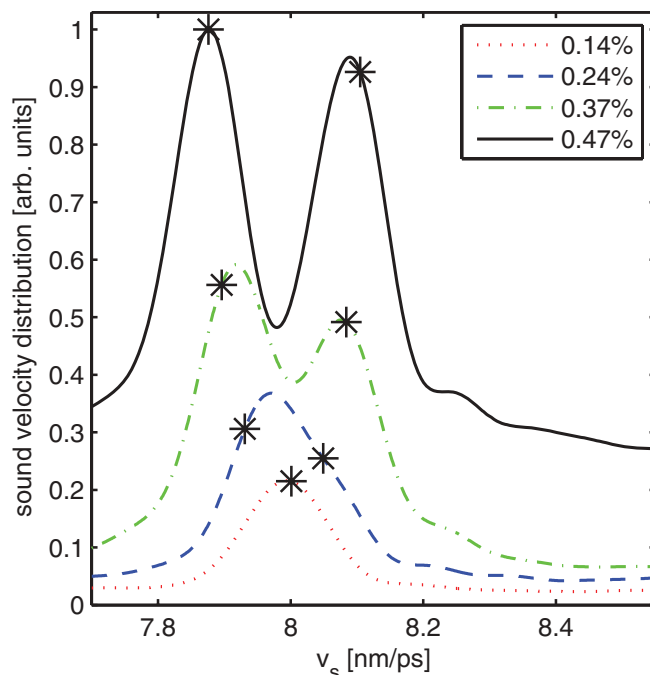


FIG. 3. (Color online) Measured sound velocity distribution of the induced strain pulse in STO. The different pump fluences were calibrated with the UXRD measurement to the resulting induced strains of the LSMO layer which is directly linked to the strain amplitude of the bipolar strain pulse in the STO. The narrow distribution for 0.14% strain implies that the entire strain pulse essentially propagates with a speed around 8 nm/ps. With increasing strain amplitude the sound velocity distribution gets broader and eventually a double-peak distribution is established. At high excitation levels different parts of the strain pulse propagate with different velocities. The stars indicate the sound velocities of the self-steepened sound pulses simulated in Fig. 4(a).

amplitude. The strain amplitude itself modulates the sound velocity of the medium.

To verify these assignments and to understand the underlying excited phonon spectrum, we simulate the lattice dynamics in a linear-chain model which was successfully tested against UXRD data in several cases.^{21,30} In addition to the model proposed in Ref. 21, we introduce an anharmonic potential between adjacent oscillators in order to describe the nonlinear wave propagation. Moreover, we add an empirical phonon damping term proportional to the velocity difference of adjacent oscillators. Mathematically the system is described by N coupled oscillators where each oscillator describes one lattice plane (half unit cell) of the LSMO thin film or the STO substrate. The set of N coupled second-order ordinary differential equations is

$$m_i \ddot{x}_i = k_M(\Delta_i - \Delta_{i-1}) + a_M(\Delta_i^2 - \Delta_{i-1}^2) + m_i \gamma_M(\dot{\Delta}_i - \dot{\Delta}_{i-1}) + F_i(t), \quad (3)$$

where $\Delta_i = x_{i+1} - x_i$ and $i = 2, \dots, N-1$. The potential is nearly harmonic with a small cubic term. This leads to the linear and parabolic force terms in the coupling force of Eq. (3), where m_i is the mass of the oscillator, k_M is the spring constant, a_M is the anharmonicity parameter, and γ_M is a material specific damping constant.^{31,32} At the interface

of LSMO and STO the differential equation is asymmetric, since k_M , a_M , and γ_M cannot be factored out as in Eq. (3). The first and the last oscillator have no opponent. This defines the boundary condition. We used $N = 48182$ oscillators, i.e., the first $9.4 \mu\text{m}$ of the STO substrate are included in the lattice dynamics simulations.

The elastic properties of LSMO and STO were taken from the literature.^{24,25} For the anharmonicity of STO we made a first approximation from the hydrostatic pressure dependence of the elastic constants, which leads directly to a qualitative agreement.² We then varied the anharmonicity of STO and LSMO to find quantitative agreement of the theory with the experimental data. The final value of the anharmonicity of STO reads $1.8 \times 10^{13} \text{ kg s}^{-2} \text{ m}^{-1}$, which is only 10% smaller than the first guess. The anharmonicity in the LSMO transducer film has only little influence on the dynamics because of the short propagation length. For this we finally used a value of $3 \times 10^{13} \text{ kg s}^{-2} \text{ m}^{-1}$. For the damping parameter γ_i we used a value which yields good agreement for phonon damping in STO observed by UXR.⁵

$F_i(t)$ describes the driving force of the oscillators due to the optical excitation process. We assume an instantaneous force step $F_i(t)$ at time zero according to the strong electron-phonon coupling in the metallic oxides.⁸ The spatial excitation profile $F_i(t)$ follows an exponential decay determined by the penetration depth of the optical pump light. Accordingly, deeper-lying unit cells exhibit less expansion.²¹

Figure 4(a) shows the simulated strain profile for different times after excitation of the sample with the smallest (black line) and largest (blue line) strain amplitude in the copropagating frame of reference. The center of the bipolar pulse which has a strain level close to zero propagates with the normal speed of sound, which is only valid in the harmonic approximation. In the regions with high amplitude the strain modulates the elastic constants. This nonlinear interaction between the masses changes the shape of the bipolar pulse, in particular leading to a self-steepening pulse front and tail. The tensile part is slower and the compressive part is faster than the sound velocity v_s of the harmonic linear chain. The speed of the pulse front propagation is read from the simulation and indicated in Fig. 3 as stars. The good agreement verifies the interpretation of the measured splitting of the sound velocity distribution.

For further comparison to the measurement and to interpret the impact of the anharmonic interaction on the classical decoupled oscillators called phonons, we analyze the simulated strain profiles in Fig. 4(a) by calculating the Fourier amplitudes $A(k_p, t)$ of sinusoidal waves composing the wave packet for each time delay t . This is essentially an amplitude of phonons (decoupled modes) which describes the wave packet. For better comparison to the experimental observable we plot A/λ in Fig. 4(c), because for a transparent medium the reflectivity modulations scale inversely with λ according to equations (35–38) in the seminal paper of Thomsen *et al.*²³ The distribution of coherently excited phonons rapidly shifts to smaller k_p vectors.

Figure 4(b) shows the amplitude of the measured Brillouin oscillations [Fig. 2(b)], which is proportional to the phonon amplitude of the phonon with wave vector k_p .²³ During the time sequence 240, 320, and 410 ps the first minimum of

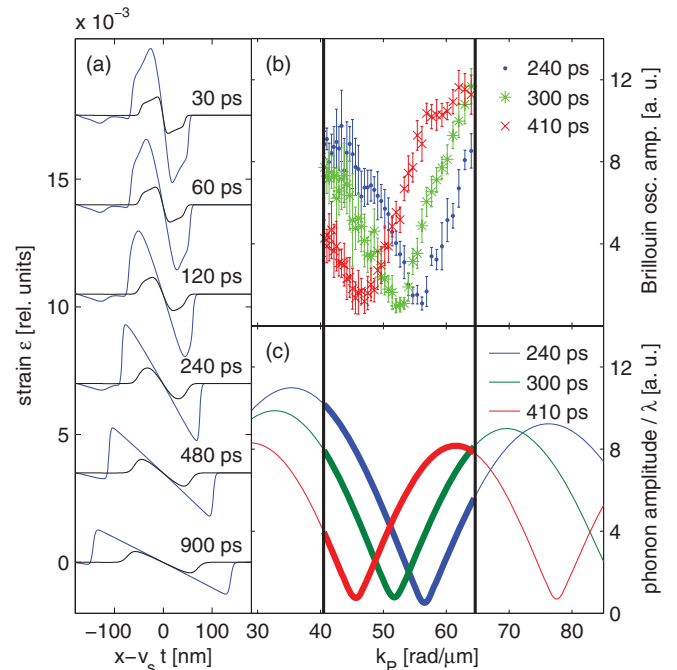


FIG. 4. (Color) (a) Spatial profile of the bipolar strain pulse in the STO for different propagation times in a frame of reference propagating with the speed of sound v_s for high amplitude (blue line, 0.47% strain) and low amplitude (black line, 0.14% strain). For large amplitude, the tensile part of the pulse propagates with subsonic speed and the compressive part propagates with supersonic speed indicated by the stars in Fig. 3. (b) Measured amplitude of oscillations for each wavelength connected to the wave vectors by the Brillouin backscattering condition. The region between the vertical black lines indicates the wave vectors that can be accessed by the optical white light. (c) Phonon amplitude divided by the wavelength λ (see text) as a function of wave vector calculated from Fourier transforms of the simulated strain profile, showing good agreement with the measurement in panel (b).

the phonon amplitude is moving through the experimental window of observation given by the Brillouin backscattering condition [Eq. (2)]. These minima represent the fact that, at a certain point in time, these phonons are not occupied. This is the fundamental interpretation of the beating of the measured oscillations. The simulation reproduces also the second measured amplitude minimum [Fig. 2(b)], which moves into the observed wavelength range about 700 ps after excitation (not shown).

We now discuss the physics behind the anharmonic linear-chain model leading to the excellent agreement of theory and experiment. Deformations are only reversible if they are infinitely slow and if the thermodynamic system is in equilibrium at any time. This is not the case for phonons which have a finite oscillation period. The phonon has to damp out because of the intrinsic irreversibility of the oscillation. In other words, the coherent phonon amplitude goes down by dissipating energy to the heat bath.^{5,9–12} In our model we consider this fact by the hydrodynamic damping term γ_M in the second line of Eq. (3).

The force term to second order in strain [a_M in Eq. (3)] is given by the anharmonic interactions of atoms which

contribute only for large strain amplitudes. The set of differential equations [Eq. (3)] can be approximated by a Korteweg–de Vries–Burgers equation (KdVB) if the phonon wavelength is much larger than the lattice constant.³³ This is advantageous to find asymptotic solutions such as solitons. Our approach is useful for the calculation of solutions with certain excitation conditions and for considering acoustic mismatches of different materials. We can account for dispersion higher than third order and compute solutions with phonon wavelengths close to the lattice constant.

In conclusion, we determined the transient phonon spectra of nonlinearly propagating strain pulses in strontium titanate

by transient reflectivity measurements for different fluences, which are experimentally calibrated by time-resolved x-ray diffraction. An anharmonic linear-chain model with phonon damping reproduces the measured spectra in a quantitative way and verifies the interpretation of the transient reflectivity measurements. The anharmonicity thus changes the phonon occupation in time and leads to compressive and tensile strain fronts traveling at 1% faster and slower speed, respectively.

We thank the DFG for supporting the project via BA 2281/3-1 and SFB 762.

*bargheer@uni-potsdam.de

¹N. D. Ashcroft, Neil W. Mermin, *Solid State Physics*, 1st ed. (Saunders College, Fort Worth, 1976).

²A. G. Beattie and G. A. Samara, *J. Appl. Phys.* **42**, 2376 (1971).

³A. Koreeda, T. Nagano, S. Ohno, and S. Saikan, *Phys. Rev. B* **73**, 024303 (2006).

⁴S. Brivio, D. Polli, A. Crespi, R. Osellame, G. Cerullo, and R. Bertacco, *Appl. Phys. Lett.* **98**, 211907 (2011); A. Devos, Y.-C. Wen, P.-A. Mante, and C.-K. Sun, *ibid.* **100**, 206101 (2012); S. Brivio, D. Polli, A. Crespi, R. Osellame, G. Cerullo, and R. Bertacco, *ibid.* **100**, 206102 (2012).

⁵M. Herzog, A. Bojahr, J. Goldshteyn, W. Leitenberger, I. Vrejoiu, D. Khakhulin, M. Wulff, R. Shayduk, P. Gaal, and M. Bargheer, *Appl. Phys. Lett.* **100**, 094101 (2012).

⁶K. G. Nakamura, S. Ishii, S. Ishitsu, M. Shiokawa, H. Takahashi, K. Dharmalingam, J. Irisawa, Y. Hironaka, K. Ishioka, and M. Kitajima, *Appl. Phys. Lett.* **93**, 061905 (2008).

⁷C. von Korff Schmising, A. Harpoeth, N. Zhavoronkov, Z. Ansari, C. Aku-Leh, M. Woerner, T. Elsaesser, M. Bargheer, M. Schmidbauer, I. Vrejoiu *et al.*, *Phys. Rev. B* **78**, 060404 (2008).

⁸A. Bojahr, D. Schick, L. Maerten, M. Herzog, I. Vrejoiu, C. von Korff Schmising, C. J. Milne, S. L. Johnson, and M. Bargheer, *Phys. Rev. B* **85**, 224302 (2012).

⁹A. Akhiezer, *J. Phys. (USSR)* **1**, 277 (1939).

¹⁰H. J. Maris, *Phil. Mag.* **12**, 89 (1965).

¹¹W. Chen, H. J. Maris, Z. R. Wasilewski, and S.-i. Tamura, *Philos. Mag. B* **70**, 687 (1994).

¹²B. C. Daly, K. Kang, Y. Wang, and D. G. Cahill, *Phys. Rev. B* **80**, 174112 (2009).

¹³P. J. S. van Capel and J. I. Dijkhuis, *Appl. Phys. Lett.* **88**, 151910 (2006).

¹⁴P. J. S. van Capel, H. P. Porte, G. van der Star, and J. I. Dijkhuis, *J. Phys.: Conf. Ser.* **92**, 012092 (2007).

¹⁵O. L. Muskens and J. I. Dijkhuis, *Phys. Rev. Lett.* **89**, 285504 (2002).

¹⁶P. J. S. van Capel and J. I. Dijkhuis, *Phys. Rev. B* **81**, 144106 (2010).

¹⁷H. Y. Hao and H. J. Maris, *Phys. Rev. B* **64**, 064302 (2001).

¹⁸H. J. Maris and S. Tamura, *Phys. Rev. B* **84**, 024301 (2011).

¹⁹G. Shirane and Y. Yamada, *Phys. Rev.* **177**, 858 (1969).

²⁰D. Schick, A. Bojahr, M. Herzog, C. von Korff Schmising, R. Shayduk, W. Leitenberger, P. Gaal, and M. Bargheer, *Rev. Sci. Instrum.* **83**, 025104 (2011).

²¹M. Herzog, D. Schick, P. Gaal, R. Shayduk, C. von Korff Schmising, and M. Bargheer, *Appl. Phys. A* **106**, 489 (2012).

²²K. Sokolowski-Tinten, C. Blome, C. Dietrich, A. Tarasevitch, M. Horn von Hoegen, D. von der Linde, A. Cavalleri, J. Squier, and M. Kammler, *Phys. Rev. Lett.* **87**, 225701 (2001).

²³C. Thomsen, H. T. Grahn, H. J. Maris, and J. Tauc, *Phys. Rev. B* **34**, 4129 (1986).

²⁴Y. H. Ren, M. Trigo, R. Merlin, V. Adyam, and Q. Li, *Appl. Phys. Lett.* **90**, 251918 (2007).

²⁵R. O. Bell and G. Rupprecht, *Phys. Rev.* **129**, 90 (1963).

²⁶M. Woerner, C. von Korff Schmising, M. Bargheer, N. Zhavoronkov, I. Vrejoiu, D. Hesse, M. Alexe, and T. Elsaesser, *Appl. Phys. A* **96**, 83 (2009).

²⁷E. Pontecorvo, M. Ortolani, D. Polli, M. Ferretti, G. Ruocco, G. Cerullo, and T. Scopigno, *APPLAB* **98**, 011901 (2011).

²⁸H. Ogi, T. Shagawa, N. Nakamura, M. Hirao, H. Odaka, and N. Kihara, *Phys. Rev. B* **78**, 134204 (2008).

²⁹M. Cardona, *Phys. Rev.* **140**, A651 (1965).

³⁰M. Herzog, D. Schick, W. Leitenberger, R. Shayduk, R. M. van der Veen, C. J. Milne, S. L. Johnson, I. Vrejoiu, and M. Bargheer, *New J. Phys.* **14**, 013004 (2012).

³¹L. D. Landau and E. M. Lifshitz, *Course of Theoretical Physics, Theory of Elasticity* (Pergamon Pr., London, 1986), Vol. 7.

³²E. Arévalo, Y. Gaididei, and F. G. Mertens, *Eur. Phys. J. B* **27**, 63 (2002).

³³E. Arévalo, F. G. Mertens, Y. Gaididei, and A. R. Bishop, *Phys. Rev. E* **67**, 016610 (2003).